C. R. Geoscience 343 (2011) 342–350

Contents lists available at ScienceDirect

Comptes Rendus Geoscience

www.sciencedirect.com

Petrology, geochemistry (Ore deposits)

Fluid inclusions and U/Pb dating of the El Pilote Fluorite skarn occurrence: Metallogenic implications

Étude d'inclusions fluides et datation U/Pb du skarn de fluorine El Pilote: implications métallogénétiques

Gilles Levresse [a,*], Jordi Tritlla [a,b], Jose Gregorio Solorio-Munguía [a], Victor Valencia [c], Porfirio Julio Pinto Linares [d]

[a] *Geofluidos, Centro de Geociencias UNAM-Campus Juriquilla, AP 1-253, Querétaro, México CP 76230, Mexico*
[b] *Repsol Exploración S.A., Paseo de la Castellana 278, 28046 Madrid, Spain*
[c] *Department of Geosciences, University of Arizona, 1040 East Fourth St, Room 510, Tucson, Arizona 85721-0077, USA*
[d] *IPICYT, Depto. Geología Económica, San Luis Potosí, S.L.P. Mexico*

ARTICLE INFO

Article history:
Received 20 January 2010
Accepted after revision 11 April 2011
Available online 24 May 2011

Presented by Zdenek Johan

Keywords:
Fluorite
Skarn
MVT
Age
Fluid Inclusions
Mexico

Mots clés :
Fluorine
Skarn
MVT
Âge
Inclusions fluides
Mexique

ABSTRACT

The "El Pilote" deposit, located in the Coahuila State (NE Mexico), is a small fluorite-bearing calcic skarn we dated at 28.4 ± 0.4 Ma (U/Pb). Fluid inclusion studies, performed on fluorite, indicate the occurrence of hot, hypersaline fluids, trapped during the prograde stage. The retrograde fluids present progressively lower temperatures and salinities. All this fluid data depicts a coherent scenario where early magmatic-dominated fluids were progressively mixed up with low-temperature, low-salinity meteoric fluids whose predominance indicates the waning of the hydrothermal system.

RÉSUMÉ

Le gisement de fluorite « El Pilote » se trouve dans l'état de Coahuila au Mexique. Il s'agit d'un petit skarn calcique daté à 28,4 ± 0,4 Ma. L'étude des inclusions fluides réalisée sur la fluorite prograde, indique la présence de fluides complexes, chauds, et très riches en sels. Les fluides rétrogrades présentent une diminution de température et de salinité. Les données d'inclusions fluides illustrent l'évolution d'un mélange entre un fluide d'origine magmatique et un fluide météorique.

1. Introduction

In northern Mexico, fluorite ore bodies are systematically located close to the limits of the Cretaceous platforms (Tritlla and Levresse, 2006) and, in some cases, near Tertiary rhyolitic hypabissal bodies (Clark et al., 1982; Kesler, 1977; Price and Henry, 1984). La Encantada-Buenavista and El Tule deposits are good examples of stratabound, basinal-brine related fluorite and celestine/fluorite mantos, respectively (Fig. 1; De Cserna (1989);

* Corresponding author.
E-mail address: glevresse@geociencias.unam.mx (G. Levresse).

1631-0713/$ – see front matter
doi:10.1016/j.crte.2011.01.006

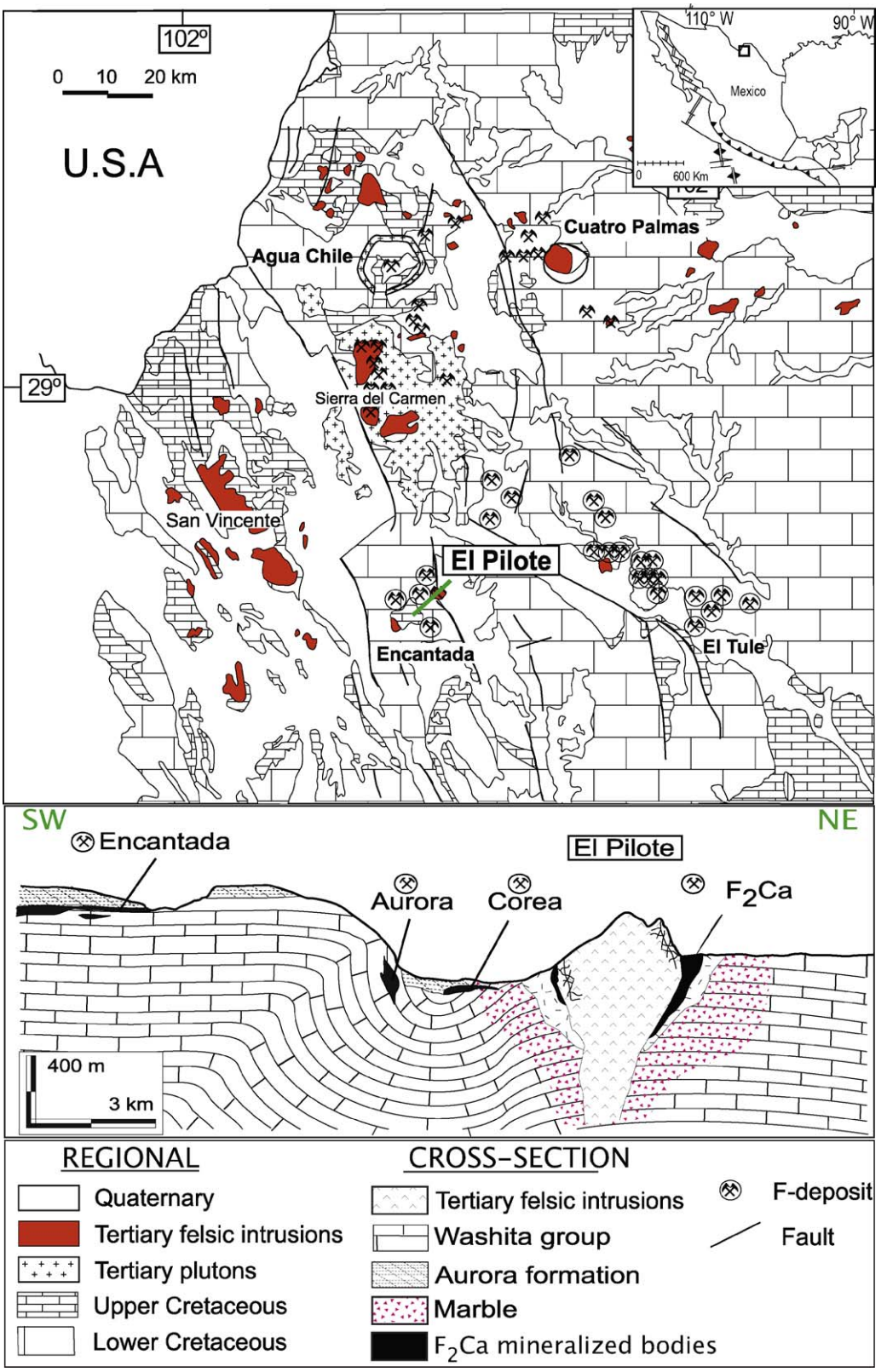

Fig. 1. (A) Geological map of northern Mexico with the location of the main fluorite deposits. (B) Geological cross-section of the El Pilote fluorite skarn; the interpreted crosscutting relationships with the La Encantada-Buenavista MVT deposits are also shown.

Fig. 1. Carte géologique du Nord du Mexique, et localisation des principaux gisements de fluorine. Coupe géologique du gisement de fluorine El Pilote.

Tritlla et al., 2007). Other carbonate-hosted deposits (Las Cuevas, San Luis Potosi, (Levresse et al., 2003); Agua Chile, Coahuila, (Levingtson, 1962)) are clearly formed after the Laramide Orogeny, are controlled by Oligocene extensional crustal faults, and are always located near or at the contact between Mesozoic carbonates and rhyolite subvolcanic bodies, clearly postdating the emplacement of the latter.

Recently, La Encantada-Buenavista fluorite district (Coahuila state, NE Mexico) has been reinterpreted as an MVT-like deposit, formed during the Laramide Orogeny, prior to Tertiary rhyolite emplacement (Tritlla and Levresse, 2006; Tritlla et al., 2007). Moreover, the Tertirary magmatic event almost exclusively resulted in the extensive recrystallization of the formerly formed fluorite mantos, with the introduction of important quantities of silica (Corea deposits in La Encantada-Buenavista Disctrict), except in one case where fragments of the fluorite deposit have been included as extensively recrystallized xenoliths within the rhyolite mass (La Azul deposit, Guerrero State; (Tritlla and Levresse, 2006)), as in a piecemeal stopping scenario.

The El Pilote deposit is a rare case of a fluorite-bearing skarn in Mexico. It is located within the La Encantada-Buenavista district, exhibiting a well-developed skarn mineral assemblage (Temple and Gronan, 1963) with small reserves (< 5 tons). The purpose of this article is to describe this unusual skarn occurrence, to discern the possible sources of fluor, as well as to find out the role of the rhyolite magmatism in the genesis of this deposit.

2. Geological setting

The oldest sequence exposed in the study area is a basal reef limestone, up to 880 m thick, locally known as the Aurora Formation (Lower Cretaceous). This unit is overlain by the Washita Group (Albian/Cenomanian), of around 130 m thick, that is subdivided into three formations: (1) Georgetown Formation (40 m of mudstone-wackestone limestone); (2) Del Rio Formation (10 m of thin-bedded shale); and (3) Buda Formation (impure limestone-fossiliferous wackestone-packstone). The Laramide Orogeny affects the entire sedimentary sequence, and developed two major folding styles: (1) asymmetrical and elongated anticline folds; and (2) domal anticlines with steep flanks.

La Encantada-Buenavista, Aurora, and Corea fluorite low temperature, stratabound, carbonate-hosted fluorite mantos are the main high tonnage deposits mined in the district (Fig. 1). The main fluorite anomaly trend spans 215 km^2 following the argillite/limestone contact of Del Rio/Buda-Aurora formations, with an average thickness of 2 m. There is a strong structural control on the distribution of fluorite bodies. They are found at the intersection of low permeability barriers with low angle faults. Fluorite appears as white to colorless, corrosion-free crystals indicative of a passive precipitation mechanism. Late cavities are filled by idiomorphic, cubic, zoned fluorite crystals with deep-purple outer zones, minor idiomorphic calcite scalenohedrons, and extremely rare barite crystals (Tritlla et al., 2007).

The Oligocene volcanism in the area is of effusive style, with abundant rhyolite necks, in contrast to the predominantly explosive style found at the Sierra Madre Occidental Volcanic Province. The Oligocene volcanics are represented by high-silica, peraluminous rhyolites, showing strong enrichment in fluorine and in some incompatible lithophile elements (Rb, La, Sm, Yb, Y, Th, U, Nb, Ta), and strong depletion in the feldspar-compatible elements Sr, Ba and Eu. This contrasts with the high-K rhyolitic rocks of the eastern Sierra Madre Occidental. Both volcanism styles and the particular chemistry are explained by a high rate of crustal extension that promoted crustal melting at high melting/segregation rates, and rapid ascent of low-viscosity fluorine-rich magmas, which inhibited melt stagnation in magma chambers (Orozco-Esquivel et al., 2002).

The emplacement of the felsic magmatic bodies, usually as volcanic dome-shaped structures and necks, are closely related to both the fault system and the fold axes. The El Pilote rhyolite is the only known fluorite-enriched volcanic neck along the entire rhyolitic intrusive trend (S. Baca, 2004, pers. com.). The El Pilote rhyolite intrudes the entire sedimentary sequence, including the fluorite mantos of the La Encantada district, and is also responsible for a subvertical metasomatic halo affecting the Aurora Formation and the Washita Group. The Tertiary magmatic felsic event produces a fluid inclusion decrepitation halo in the fluorite when the rhyolite bodies crosscut the stratabound fluorite mineralization (Tritlla et al., 2007).

3. El Pilote intrusion composition

The El Pilote rhyolite neck is characterized by a well-defined, concentric magmatic foliation, with aphanitic texture, corresponding to a hypo-abyssal body emplaced at near surface conditions. This magmatic body is composed by phenocrysts of K-feldspar, plagioclase and quartz, with a banded, whitish glassy matrix. Neither fluorite nor topaz was found as a free mineral within the matrix.

Whole rock and fluorite samples were analyzed for major and trace elements at the *Service d'Analyse des Roches et des Matériaux* of the CRPG-CNRS at Nancy (France). The rhyolitic composition has been confirmed by whole rock chemical analysis ($SiO_2 = 76.8\%$; $K_2O = 4.4\%$; and $K_2O/Na_2O = 1.2$). The F-saturation in the melt was determined for a temperature of 850 ± 15 °C (Scaillet and Macdonald, 2004), the latter calculated with the zircon saturation thermometer (Hanchar and Watson, 2003). Fluorine saturation is then estimated around 0.26%.

Chondrite-normalized REE composition of the El Pilote rhyolite shows a flat pattern with a $(La/Yb)_N = 3.32$, a pronounced depletion in Eu ($Eu/Eu^* = 0.06$) and beryllium enrichment identical to anomalous (F-Li-Be-rich) rhyolites already described in Mexico (Orozco-Esquivel et al., 2002).

4. U/Pb geochronologic constraints

Zircons recovered from the El Pilote intrusion were carefully selected for dating. Analyses were carried out at the University of Arizona (V.A. Valencia, analyst) using a LA-ICPMS Micromass Isoprobe. Analyzed zircons were small (< 100 microns) and prismatic or needle-shaped. They show a regular magmatic zoning and have no inherited cores or inclusions. Nineteen analyses provided

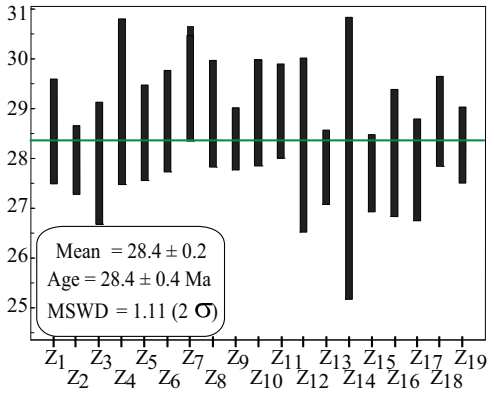

Fig. 2. LA-ICPMS $^{206}Pb/^{238}U$ zircon ages (Z_1 to Z_{19}) for the El Pilote rhyolite. The weighted mean age is calculated with the Isoplot program (Bakker, in press). Errors represent analytical precision at 2 sigma.

Fig. 2. Âges $^{206}Pb/^{238}U$ (monocristal de zircon ; LA-ICP-MS) de la roche intrusive rhyolitique El Pilote. L'âge moyen est calculé par le logiciel Isoplot (Bakker, sous presse). Les erreurs représentent la précision analytique à 2 sigma.

$^{206}Pb/^{238}U$ ages dispersed between 27.7 ± 0.8 Ma and 29.6 ± 1.1 Ma (Fig. 2; Table 1). The weighted mean crystallization age of zircons from the El Pilote rhyolitic intrusion is calculated according to Ludwig (2003) at 28.4 ± 0.4 Ma ($n = 19$; MSWD = 1.11).

5. Skarn characteristics: alteration and mineralization

The fluorite mineralization at El Pilote occurs in a skarn developed vertically around the margins of the rhyolite neck. The endoskarn is poorly represented (a few centimeters wide), whereas the exoskarn formed within the host limestones and reaches up to 200 m in thickness. Hydrothermal alteration is controlled by north-south trending faults, bedding planes, and reactive rocks of the Aurora and Buda formations.

This skarn is made up by a lateral succession of: (1) an inner rhyolite neck; (2) an endoskarn composed of zoned garnet (from Adr_{100} to $Adr_{20}Grs_{70}Py_{10}$), wollastonite (Wo_{100} to $Wo_{50}En_{50}$), calcite, and green fluorite; (3) an exoskarn, several hundred meters thick, composed mainly by recrystallized calcite, proximal green and distal white fluorite, pyroxenoid ($Wo_{50}En_{50}$ to $Wo_{50}En_{30}Fs_{20}$; Fig. 3), garnet (from Adr_{100} to $Adr_{20}Grs_{80}$; Fig. 3), spurrite ($(Ca_5SiO_4)_2(CO_3)$), rankinite ($Ca_3Si_2O_7$), albite, tremolite, Mn-calcite, and ilvaite ($CaFe_3O\ Si_2O_7\ (OH)$); and (4) an outer marble aureole, consisting of a foliated, manganiferous marble (with braunite and hausmannite) in which the mineralogical zoning is roughly parallel to the rhyolite contact, progressively grading outwards to the well preserved reefal limestone. This marble contains irregular and small patches of garnet, possibly reflecting original compositional inhomogeneities within the limestone.

The skarn system (endoskarn and exoskarn) is crosscut by a retrograde assemblage following fractures, represented by a limited propylitic alteration, with tremolite, sericite, quartz, calcite and a swarm of fluorite veins (Fig. 3). Purple-colored, retrograde fluorite occurs mainly enclosed within the rhyolite neck (with very minor quantities in the exoskarn) while white fluorite is solely present as a retrograde phase within the exoskarn. Sulfides have been detected neither within the prograde metasomatic event nor in the retrograde alteration episode.

One remarkable characteristic of this skarn is that fluorite only appears as minute octahedral crystals, both in the prograde (green) and retrograde (purple and white) events, lacking more complex (dodecahedrons) or usual (cubic) crystal shapes. Fluorite octahedron faces at El Pilote always have very rough surfaces, indicative of very rapid, almost skeletal growth. Fluorite octahedrons (skeletal growth) are characteristically found in the early stages of

Table 1
U/Pb isotopic data for single zircon crystal from El Pilote intrusives obtained by LA-ICPMS.

Tableau 1
Données isotopiques U/Pb réalisées sur monocristal de zircon par LA-ICPMS de la roche intrusive rhyolitique El Pilote.

Sample	U (ppm)	Th (ppm)	U/Th	$^{206}Pb/^{204}Pb$	$^{206}Pb/^{238}U$ ratio	± (%)	APPARENT AGES	
							$^{206}Pb/^{238}U$	± (Ma)
Z_1	409	205	2.0	602	0.00444	3.69	28.5	1.1
Z_2	583	343	1.7	912	0.00435	2.47	28.0	0.7
Z_3	483	279	1.7	559	0.00434	4.40	27.9	1.2
Z_4	459	272	1.7	805	0.00453	5.72	29.1	1.7
Z_5	413	222	1.9	589	0.00443	3.37	28.5	1.0
Z_6	556	309	1.8	1297	0.00447	3.56	28.7	1.0
Z_7	423	229	1.9	830	0.00460	3.59	29.6	1.1
Z_8	421	266	1.6	847	0.00449	3.71	28.9	1.1
Z_9	615	467	1.3	2138	0.00441	2.21	28.4	0.6
Z_{10}	667	575	1.2	429	0.00449	3.69	28.9	1.1
Z_{11}	608	262	2.3	856	0.00450	3.27	28.9	0.9
Z_{12}	455	266	1.7	319	0.00439	6.20	28.3	1.7
Z_{13}	544	281	1.9	1061	0.00433	2.69	27.8	0.7
Z_{14}	438	234	1.9	480	0.00435	10.12	28.0	2.8
Z_{15}	663	541	1.2	425	0.00431	2.80	27.7	0.8
Z_{16}	430	219	2.0	556	0.00437	4.57	28.1	1.3
Z_{17}	169	169	1.0	226	0.00432	3.70	27.8	1.0
Z_{18}	463	237	2.0	374	0.00447	3.16	28.7	0.9
Z_{19}	549	294	1.9	1225	0.00439	2.71	28.3	0.8

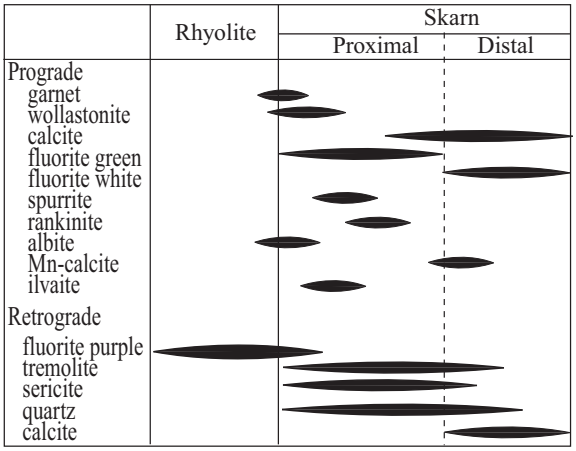

Fig. 3. Paragenetic sequence of the El Pilote deposit.

Fig. 3. Séquence paragénétique du gisement de fluorine El Pilote.

formation in hydrothermal ore deposits, while dodecahedrons are relatively frequent intermediate shapes and cubes are the main, late crystal forms (Glikin, 2009).

6. Fluid inclusion studies

A fluid inclusion study was carried out on both the prograde (green fluorite) and retrograde (white and purple fluorite) alteration events. Fluid inclusion microthermometric results are presented in Figs. 4 and 5 and Table 2. Twenty double-polished fluorite wafers were selected for microthermometric analysis ($n = 174$). These were performed using a Linkam THMSG-600 heating-freezing stage, calibrated with synthetic fluid inclusions, the triple point of pure water (0.0 °C), the triple point of CO_2 in pure CO_2-bearing fluid inclusions (−56.6 °C), and chemicals of known melting point from the Merck Corporation. Accuracy is estimated at about ±0.2 °C for cooling runs and ± 2 °C for heating runs.

The wafers used for the fluid inclusion work were obtained for every single fluorite generation found, both prograde and retrograde, including all the colors observed. Moreover, special care was taken in selecting defect-free fluorite crystals, with no visible evidences of deformation. In all the selected samples fluid inclusions assemblages are conformed by primary fluid inclusions, either isolated or along growth zones, as well as pseudosecondary and secondary fluid inclusions trapped along fracture planes.

6.1. Fluid inclusion types and distribution

It is remarkable that all prograde fluorite crystals show a plethora of primary fluid inclusion types arranged within different FIA's, while retrograde fluorite presents only one type of fluid inclusions (both primary and secondary). All these fluid inclusions are found either isolated or in small clusters and mostly display well-developed tetrahedral crystal shapes. Four fluid inclusions types have been found: (1) very rare (< 5%), monophase, vapor-rich fluid (V) inclusions without any observable liquid phase; (2) two-phase (L + V), liquid-rich inclusions; (3) supersaturated, polyphase fluid inclusions, with two daughter (cubic halite and rounded sylvite crystals) and several trapped minerals (calcite, rutile and two unidentified phases); and (4) undersaturated, polyphase fluid inclusions, with several trapped minerals (calcite, rutile and two unidentified phases; Fig. 4). All the solid phases present in the fluid inclusions were tentatively identified by the combination of petrography, microthermometry and Raman spectrometry analyses. Finally, all the studied fluid inclusions present low to very low CH_4 and CO_2 contents (determined by Raman microprobe).

6.1.1. Fluid inclusions in prograde fluorite

As stated before, type 1, vapor-rich fluid inclusions could not be studied as no liquid-rich rim was seen to be formed after the freezing runs, most probably due to optical limitations coupled with the fluorite high refraction index.

Type 2 fluid inclusions show homogenization temperatures (Th), by bubble shrinkage, ranging from +141 to +238 °C. Eutectic temperatures were very difficult to obtain due to optical limitations, but they seem to be at fairly low temperatures around − 50 °C, indicating the presence of $CaCl_2$. Subsequent melting of a high-relief phase, identified as hydrohalite, occurs at temperatures between −28.6 and 22.7 °C; finally ice melted at temperatures between −12.8 and −7.8 °C. The calculated total salinity (Oakes et al., 1990) spans from 6.3 a 16.4 wt% eq NaCl, where $CaCl_2$ contents are calculated to be between 0.3 a 6.2 wt%.

Poly-phase type 4 fluid inclusions show homogenization temperatures (Th), by bubble shrinkage, ranging from +235 to +424 °C. Eutectic temperatures were very difficult to obtain due to optical limitations, but they seem to be at fairly low temperatures around −50 °C, indicating the presence of $CaCl_2$. Subsequent melting of a high-relief phase, identified as hydrohalite, occurs at temperatures between −39.5 and −23.1 °C; finally ice melted at temperatures between −18.4 and −11.5 °C. The calculated total salinity (Bakker, in press) spans from 15.5 a 21.8 wt% eq NaCl, where $CaCl_2$ contents are calculated to be between 3.1 and 6.2 wt%, very similar to the salinities calculated for type 2 fluid inclusions. KCl content in both type 2 and 4 fluid inclusions is mostly possible but undetectable under microthermometric studies, so its concentration was considered negligible in these fluid inclusion types.

Poly-phase, hypersaline type 3 fluid inclusions were studied only by heating runs. Sylvite, present as rounded cubic crystals, was the first phase to be dissolved at temperatures between +23.4 and +27.7 °C, with KCl calculated salinities between 4.1 to 4.9 wt%; halite crystals solubilized at temperatures between +122.0 and +151.7 °C, with calculated NaCl salinities between 22.1 to 22.9 wt%. Total salinities, calculated (Bakker, in press), are very constant, and between 31.7 and 32.5 wt% eq. of NaCl. Finally, total homogenization by bubble shrinkage took place at temperatures between +160 and +325 °C.

It is interesting to note that the fluid inclusion type abundances vary with the distance to rhyolite. Prograde fluorite in close contact with the intrusive neck present, type 1 (vapor-rich) and type 3 (supersaturated) exclusively;

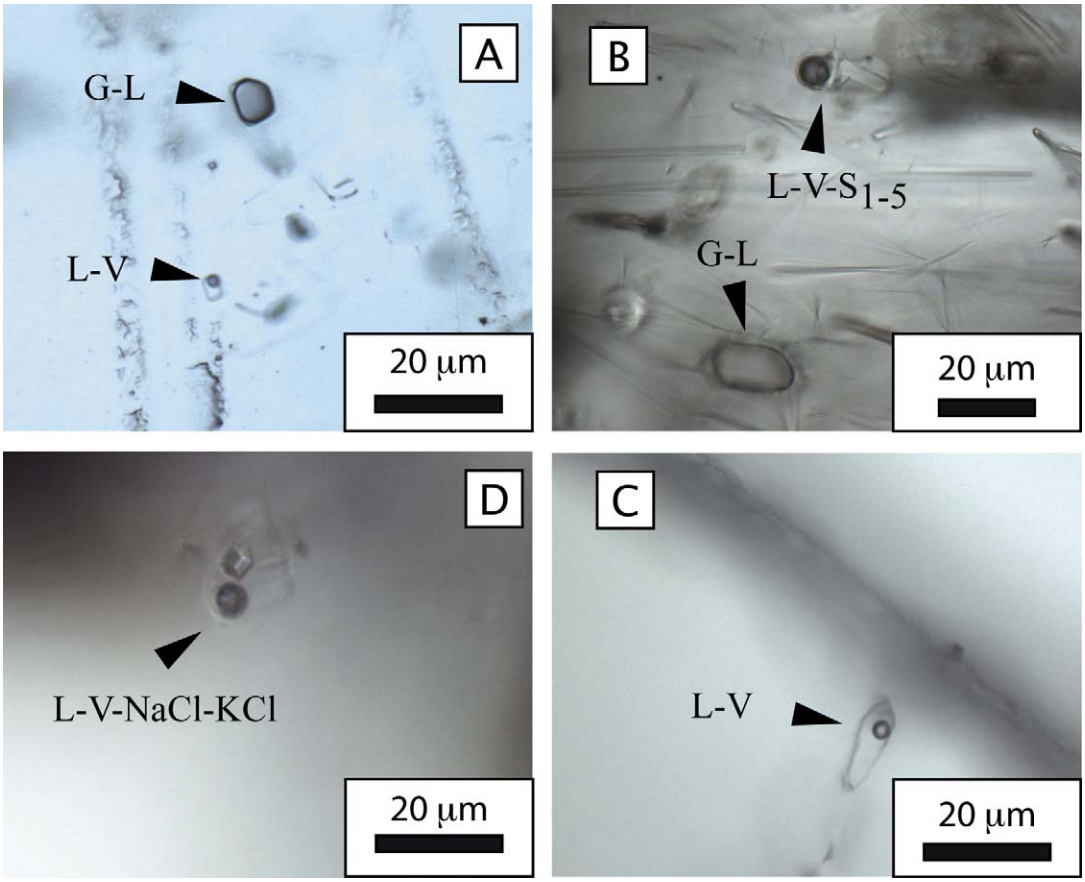

Fig. 4. (A) Heterogeneous trapping in prograde green fluorite. Two-phase fluid inclusions (G; type 1) and (L-V; type 2); (B) Heterogeneous trapping in prograde green fluorite. Two-phase and multi-phase fluid inclusions (G; type 1) and (L-V-S; type 4); (C) Multi-phase fluid inclusion (L-V-NaCl-KCl; type 3) in green prograde fluorite; (D) Two-phase fluid inclusion (L-V) in white retrograde fluorite.

Fig. 4. (A) Piégeage hétérogène dans une fluorine verte prograde. Inclusions fluides biphasées (G ; type 1) et (L-V ; type 2). (B) Piégeage hétérogène dans une fluorine verte prograde. Inclusions fluides biphasées et multi-phasées (G ; type 1) et (L-V-S ; type 4) ; (C) Inclusion fluide multi-phasée (L-V-NaCl-KCl) dans une fluorine verte prograde ; (D) Inclusion fluide biphasée (L-V) dans une fluorine blanche rétrograde.

prograde fluorite crystals sampled within a meter or so from the rhyolite neck presents rare type 4 and abundant secondary type 2 fluid inclusions.

Secondary, type 2 fluid inclusions in prograde fluorite are always located within exfoliation planes and show very variable liquid-to-vapor ratios probably due to of necking-down process. As a consequence, they were carefully avoided for microthermometric purposes.

6.2. Fluid inclusions in retrograde fluorite

Retrograde fluorite within both the rhyolite and the outer enclosing carbonate presents exclusively type 2 fluid inclusions. One of the most striking features found in this deposit is an empiric correlation between the color of the retrograde fluorite (early purple; late white) and their primary fluid inclusion characteristics.

Purple-colored retrograde fluorite is found both within the rhyolite and the enclosing marble aureola. Type 2, primary and pseudo-secondary fluid inclusions trapped within this purple fluorite show a wide size range (10 to > 100 μm) and variable shapes (globular, negative crystals or irregular). These fluid inclusions present consistent vapor/liquid ratios ($\sim$0.2) and are devoid of CH_4, CO_2 and daughter or trapped crystals.

The fluid inclusions trapped in purple fluorite within the rhyolite neck, present homogenization temperatures by bubble shrinkage between 179 to 182 °C (Fig. 5). Eutectic temperatures are very difficult to measure due to the minute size of the fluid inclusions, but seem to be compatible with a NaCl-dominated fluid (around −21 °C). Ice melting temperatures are recorded to occur between −11.6 to −10 °C, with corresponding salinities of 13.6 to 15.6 wt% eq. of NaCl (Fig. 5).

Type 2 fluid inclusions in limestone-enclosed purple fluorite present homogenization temperatures by bubble shrinkage between 174 and 176 °C, slightly lower than their rhyolite-enclosed counterparts (Fig. 5). Ice melting occurs around −1.4 °C, corresponding to salinites of 2.2 wt% eq. of NaCl (Fig. 5).

Late, white-colored retrograde fluorite is found exclusively within the outer marble aureola, and contains exclusively type 2 bi-phase (L + V) fluid inclusions. They are minute, mostly below 5 μm in diameter with very rare,

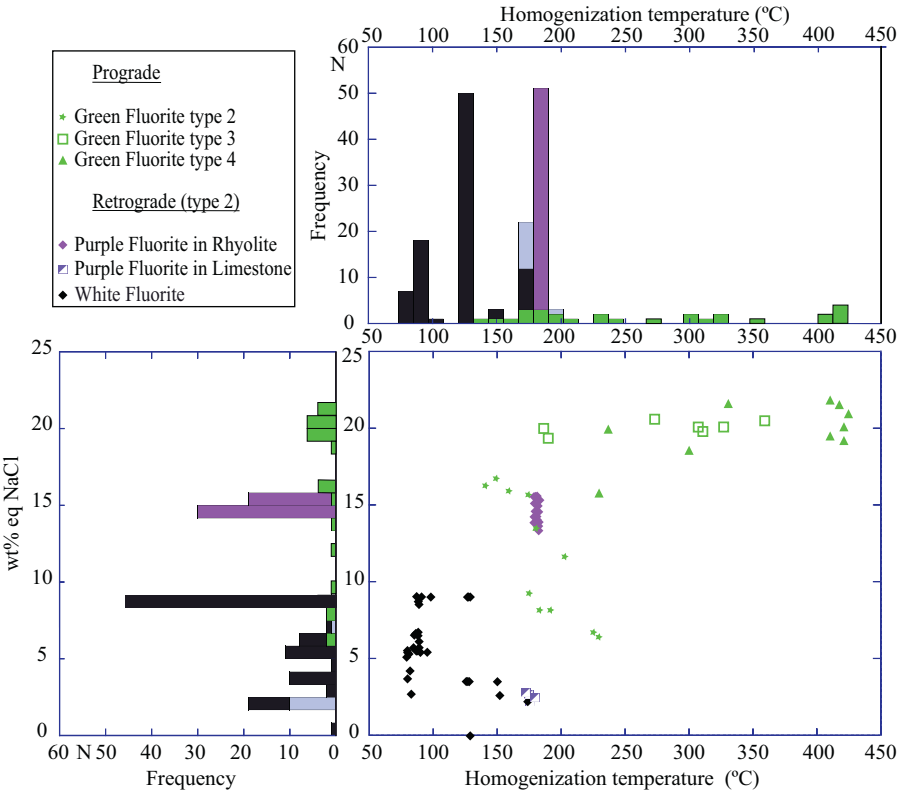

Fig. 5. Temperature vs. salinity plot for all the fluid inclusion generations. For further information see discussion. Salinity and homogenization temperature histograms for aqueous inclusions from El Pilote. Green: prograde event; black and purple: retrograde event.

Fig. 5. Diagramme de la température en fonction de la salinité des diverses générations d'inclusions fluides analysées. Histogrammes de salinité et de température d'homogénéisation des inclusions fluides de El Pilote. En vert : l'événement prograde ; en noir et violet : l'événement rétrograde.

Table 2
Temperature and salinity synthetic data of prograde and retrograde samples from El Pilote skarn fluorite deposits. Tms_{2-4-5}: melting temperature of undetermined solids 2-4-5. Errors on meditions are 0.2 °C.

Tableau 2
Données synthétiques de température et de salinité des échantillons progrades et rétrogrades étudiés dans le gisement de fluorine El Pilote. Tms_{2-4-5} : température de fusion des solides non déterminés 2-4-5. Les erreurs sur les mesures sont de 0,2 °C.

Event	Minerals	Inclusion type	Inclusion number	Th range	Tf range	Wt% NaCl range	Tmi hydrohalite	Wt% CaCl2 range
Prograde in limestone	Fluorite green	Type 2	11	141 to 238	−12.8 to −7.8	6.3 to 16.4	−28.6 to −22.7	
Prograde in limestone	Fluorite green	Type 2	11	Tm sylvite	Tms2	Tm Halite	Tms4	Tms5
				Th range	Tf range	Wt% NaCl range	Tmi hidrohalite	Wt% KCl range
Prograde in limestone	Fluorite green	Type 3	7	160 to 352	−12.3 to −8.8	19.6 to 20.4	−28.1 to −22.6	11.3 to 12.9
				Tm sylvite	Tms2	Tm Halite	Tms4	Tms5
Prograde in limestone	Fluorite green	Type 3	7	23.4 to 27.7		122.2 to 151.7		
				Th range	Tf range	Wt% NaCl range	Tmi hidrohalite	Wt% CaCl2 range
Prograde in limestone	Fluorite green	Type 4	10	235 to 423	−18.4 to −11.5	15.5 to 21.8	−39.5 to −23.1	3.1 to 6.2
				Tm sylvite	Tms2	Tm Halite	Tms4	Tms5
Prograde in limestone	Fluorite green	type 4	10	23.4 to 27.7	35.6 to 41.7	122.2 to 151.7	210.5 to 251.8	406.4 to 422.9
				Th range	Tf range	Wt% NaCl range	Tmi hidrohalite	Wt% CaCl2 range
Retrograde in limestone	Fluorite purple	Type 2	11	174 to 176	−1.3 to −1.4	2.2 to 2.3		
Retrograde in rhyolite	Fluorite purple	Type 2	44	179 to 182	−11.6 to −10	13.9 to 15.7		
Retrograde in limestone	Fluorite white	Type 2	86	79 to 174	−6 to −1.4	2.2 to 9.1		

big inclusions (< 50 μm) Homogenization occurs into the liquid phase at temperatures between 79 to 174 °C (Fig. 5). Ice melting temperatures range between −6 °C to −1.4 °C, corresponding to salinities between 2 and 9 wt% eq. of NaCl (Fig. 5).

7. Discussion

The El Pilote rhyolite chemistry is similar to the topaz-bearing rhyolites previously described in Mexico (Orozco-Esquivel et al., 2002) and in the USA, (Bodnar, 1993; Christiansen et al., 1983; Price and Henry, 1984), although neither free topaz nor free fluorspar were observed as rock-forming minerals.

The U-Pb age determined for the El Pilote rhyolite appears to be in good agreement with both the crosscutting relationships seen in the field and with the previous reported ages of comparable rhyolite intrusions related to F-anomalies in Coahuila (Cantegrel and Robin, 1979) and in northern Mexico (San Miguelito and Chinchindaro, K-Ar on biotite (Cantegrel and Robin, 1979); El Realito, El Refugio, K-Ar, whole rock (Labarthe-Hernandez et al., 1982; Tuta et al., 1988); Zapote, Cantera, Cuatralba, K-Ar on sanidine, (Orozco-Esquivel et al., 2002)). The results of U-Pb dating on zircon constrain both the age of the emplacement of the Pilote rhyolitic neck (28.4 ± 0.4 Ma) and, indirectly, the hydrothermal alteration related system.

The octahedral crystal habit of fluorite is influenced both by its internal structure and the conditions prevailing during the growth processes, as temperature, pH value, Ca/CO_2 concentration of the solutions and fluorine super-saturation (Zidarova, 1978, 1989), as well as the growth velocity and nucleation (Kostov, 2002). The presence of octahedral crystals during all process (from prograde green fluorite to retrograde white fluorite) suggests a continuum of the physico/chemical conditions.

Fluid inclusions trapped in prograde fluorite records a complex fluid history. Primary high temperature type 4 and, possibly, type 2 fluid inclusions trapped in prograde fluorite are interpreted to represent aliquots of a rhyolite-equilibrated fluid, regardless of its origin (either ortho-magmatic, meteoric or a mixture). The emplacement of the subvolcanic rhyolite neck furnished the heat needed for the hydrothermal system to operate. Boiling, recorded in prograde fluorite, was triggered by both the heat supplied and the decompression of the whole system during magma ascent, with subsequent fluid mixing with surficial waters. Flashing during boiling originated types 1 (vapor-rich) and types 3 (with trapped minerals) and 4 (NaCl and KCl-bearing, with trapped minerals) fluid inclusions to form, as fluorite precipitated trapping heterogeneous fluids. Boiling accounts for a super-saturation and rapid growth of skeletal fluorite crystals, prevailing the octahedral facies over more evolved crystals facies (dodecahedrons, cubes), as discussed above.

Fluid inclusions in late, retrograde octahedral purple and white fluorite present a path towards low temperature and (NaCl-dominated) salinity, suggesting the influx of meteoric water, still scavenging small quantities of fluor from the rhyolite zone towards the outer limestone, during the waning of the hydrothermal system.

The source of fluor remains problematic. Two possible fluor origins can be invoked: (1) a preconcentration of fluor as a volatile due to a very-low degree of melting of the parent rock, prior to its ascent and emplacement, giving rise to a volatile-rich, rhyolitic melt (Christiansen et al., 1983; Price, 2004; Price and Henry, 1984); (2) the remobilization of fluor from the regional rocks (and probably the close fluorite mantos neerby) during the melt ascent, until the PTX conditions of fluorite precipitation are reached (Richardson and Holland, 1979).

The El Pilote rhyolitic intrusion presents a very low F^- concentration (less than 0.3%) compared to the F^- rich volcanic or haplogranite system at similar temperature (from 0.8 to 3.6 wt% CaF_2 (Dolejš and Baker, 2006)). Hence, the F low concentration in the melt suggests that an external source must be invoked. Based on the knowledge of the local geology, the low F^- saturation of the rhyolite, the fluid temperature and chemistry of the paleofluids, the only plausible source for the F appears to be the locally available stratabound fluorite mantos. The predominance of octahedral shapes in skarn fluorite, suggests that fluorite formed very rapidly in a very short time. The geological evidences place the stratabound carbonate-hosted fluorite deposits almost at the same stratigraphical level than the rhyolite neck. Hence, we suggest that a remobilization between the rhyolite intrusion and the preexisting fluorite mantos was the main mechanism that originated such an unusual fluorite concentration.

8. Conclusions

El Pilote fluorite deposit was generated by the intrusion of a rhyolite body at 28.4 ± 0.4 Ma, that developed an infiltrative calcic skarn, with a reduced endoskarn, and a well developed exoskarn zone. The dating of the emplacement of the El Pilote rhyolite indirectly dates the hydrothermal system.

The well-developed exoskarn shows a metasomatic column with inner garnet and outer prograde (green) fluorite passing to a highly recrystallized carbonate (marble). A widespread, mineralized stockwork represents the retrograde event with purple-colored fluorite exclusively present within and around the rhyolitic neck; white fluorite appears as a retrograde distal phase within the stockwork affecting the carbonates. In all cases, minute octahedral fluorite is dominant, suggesting a very rapid (skeletal) crystal growth.

Fluid inclusion data gathered on prograde fluorite indicates the dominance of hot (170 to > 400 °C) and saline to hypersaline fluids in this stage (from 6.3 to 32.5 wt% eq. NaCl). After the fluid inclusions assemblages found, boiling is thought to be the main mechanism of fluid evolution and fluorite nucleation and precipitation. This is mineralogically supported by the sole presence of fluorite octahedra throughout the prograde stage. The fluids in retrograde fluorite evolved progressively towards lower temperatures (from 182 to 79 °C) and salinities (from 15.7 to 0.1 wt% eq. NaCl). All this fluid data depicts a coherent scenario where firstly magmatic-equilibrated fluids boiled off and progressively mixed up with low-temperature, low-salinity

meteoric fluids, until the cessation of the hydrothermal fluid circulation and mineralization.

Acknowledgements

The Fluorita de Mexico Mining Corporation is thanked for the logistical field assistance. This study was funded by scientific projects UNAM IN100707 and CONACYT 81584 to G.L. and UNAM IN114002, IN114106 and CONACYT 49234-F to J.T. Jerome Demange is thanked for the analyses performed in the Electron Probe facilities at the UHP, Nancy, France. Victor Valencia and the University of Arizona provided U-Pb zircon analysis.

References

Bakker, R., in press. Package fluids, part 4: thermodynamic modeling and purely empirical equation for H_2O-NaCl-KCl solutions. Geochim. Cosmochim. Acta.

Bodnar, R.J., 1993. Revised equation and table for determining the freezing point depression of H_2O–NaCl solutions. Geochim. Cosmochim. Acta 57, 683–684.

Cantegrel, J., Robin, C., 1979. K-Ar dating of the eastern Mexican volcanic rocks and relation between andesitic and alkaline provinces. J. Volc. Geophys. Res. 5, 99–114.

Christiansen, E.H., Burt, D.M., Sheridan, M., Wilson, R.T., 1983. The petrogenesis of topaz rhyolites from the western United States. Contrib. Mineral. Petr. 83, 16–30.

Clark, K.F., Foster, C.T., Damon, P.E., 1982. Cenozoic mineral deposits and subduction related magmatic arcs in Mexico. Geol. Soc. Am. Bull. 93, 533–544.

De Cserna, Z., 1989. An outline of the geology of Mexico. In: Bally, A.W., Palmer, A.R. (Eds.), The Geology of North America-An Overview. Geol. Soc. Am. Mem. 233–264.

Dolejš, D., Baker, R.D., 2006. Fluorite solubility in hydrous haplogranitic melts at 100 Mpa. Chem. Geol. 225, 40–60.

Glikin, A.E., 2009.In: Polymineral-Metasomatic Crystallogenesis. Springer (314 pp. I).

Hanchar, J.M., Watson, E.B., 2003. Zircon Saturation Thermometry. Rev. Mineral. Geochem. 53, 89–112.

Kesler, S.E., 1977. Geochemistry of manto fluorite deposits, northern Coahuila, Mexico. Econ. Geol. 72, 204–218.

Kostov, A., 2002. Crystal-morphological evolution of minerals. The 4th scientific discovery in Bulgaria. Bulg. Miner. Soc.

Labarthe-Hernandez, G., Triatan-Gonzalez, M., Aranda-Gomez, J.J., 1982. Revision estratigrafica del Cenozoico de la parte central del estado de San Luis Potosi, 85. Instituto Geologia, Folleto tecnico, Universidad Autonoma San Luis Potosi, 208 p.

Levingtson, A.A., 1962. Beryllium-fluorine mineralization at Aguachile Mountain. Coahuila. Mexico. Am. Mineral. 47, 67–75.

Levresse, G., Gonzalez-Partida, E., Tritlla, J., Camprubi, A., Cienfuegos-Alvarado, E., Morales-Puente, P., 2003. Fluid origin of the world-class, carbonate-hosted Las Cuevas fluorite deposit (San Luis Potosi, Mexico). J. Geochem. Explor. 78-79 537–543.

Ludwig, K.J., 2003. Isoplot 3. 00, 4. Special Publication, Berkeley Geochronology Center, 70 p.

Oakes, C.S., Bodnar, R.J., Simonson, J.M., 1990. The system NaCl-$CaCl_2$-H_2O: the ice liquidus at 1 atm total pressure. Geochim. Cosmochim. Acta 54, 603–610.

Orozco-Esquivel, M.T., Nieto-Samaniego, A.F., Alaniz-Alvarez, S.A., 2002. Origin of rhyolitic lavas in the Mesa Centralm, Mexico, by crustal melting related to extension. J. Volc. Geoth. Res. 118, 37–56.

Price, J.G., 2004. I never met a rhyolite I didn't like-some of the Geology in Economic Geology. SEG Newsletter 57, 1–13.

Price, J.G., Henry, C.D., 1984. Stress orientations during Oligocene volcanism in Trans-Pecos Texas: timing the transition from Laramide compression to Basin and Range tension. Geology 12, 241–389.

Richardson, C.K., Holland, H.D., 1979. Fluorite deposition in hydrothermal systems. Geochim. Cosmochim. Acta 43, 1327–1335.

Scaillet, B., Macdonald, R., 2004. Fluorite stability in silicic magmas. Contrib. Mineral. Petr. 147, 319–329.

Temple, A.K., Gronan, R., 1963. Manto deposits of fluorspar, northern Coahuila, Mexico. Econ. Geol. 58, 1037–1053.

Tritlla, J., Levresse, G., 2006. Comments to "(U-Th)/He dating of fluorite: application to the La Azul fluospar deposit in the Taxco mining district, Mexico" (Min. Dep., 39, 976–982) by Pi et al. Min. Deposita 41, 296–299.

Tritlla, J., Levresse, G., Corona-Esquivel, R., Banks, D., Lamadrid, H., Bourdet, J., 2007. Epigenetic, Low-temperature, carbonate-hosted Pb-Zn-Cu-Ba-F-Sr deposits in Mexico: a Mississippi Valley-Type classification. GSA Special Paper 422, 417–432.

Tuta, Z.H., Sutter, J.F., Kesler, S.E., Ruiz, J., 1988. Geochronology of mercury, tin and fluorine mineralization in northern Mexico. Econ. Geol. 83, 1931–1942.

Zidarova, B.P., 1978. Hydrothermal synthesis of fluorite. Geochem. Miner. Petrol. 8, 27–36.

Zidarova, B.P., 1989. Mineralogical Peculiarities and Genesis on Fluorite in the Industrial Deposits in Bulgaria. – PhD thesis, Sofia, Bulgarian Academy of Science, 287 p.